Frequency-Based Wind Gust Estimation for Quadrotors Using a Nonlinear Disturbance Observer

Abner Asignacion, Jr, Satoshi Suzuki, *Member, IEEE*, Ryusuke Noda, Toshiyuki Nakata, and Hao Liu

***Abstract*—In city-wide weather prediction, wind gust information can be obtained using unmanned aerial vehicles (UAVs). Although wind sensors are available, an algorithm-based active estimation can be helpful not only as a weightless substitute but also as feedback for robust control. This paper aims to estimate the wind gusts affecting the quadrotors (a type of UAV) as the input disturbances by using a frequency-based nonlinear disturbance observer (NDOB). To obtain highly accurate estimations, frequency is considered as the main design parameter, thereby focusing the estimation on the frequency range of the wind gusts. The NDOB is developed using the Takagi-Sugeno (T-S) fuzzy framework. In this approach, the twelfth-order nonlinear model is approximated into a sixth-order T-S fuzzy model to reduce computational cost. A two-step verification method is presented, which includes MATLAB/Simulink simulations and the experiments performed using a 2.5 kg quadrotor.**

***Index Terms*—Aerial Systems: Applications, aerial systems: mechanics and control, disturbance observer, fuzzy.**

I. Introduction

RECENTLY, the development of unmanned aerial vehicles (UAVs) has become an active research field because they have both commercial and scientific applications, such as environmental monitoring, forestry, and weather prediction [1]. UAVs have been used for large-scale hurricane prediction as well as citywide forecasting, and their sizes vary from simple kites that are equipped with a thermometer to small UAVs and weather drones. They capture various atmospheric data such as wind speed, direction, temperature, and pressure.

For citywide weather prediction, small UAVs such as quadrotors are required to obtain the necessary atmospheric data from the ground surface, up to a height of hundred meters. Thermometers, pressure sensors, flow sensors, and anemometers can be mounted on the quadrotor body to measure the atmospheric data. However, these sensors add to the weight of the UAVs and change their inertia, thereby limiting their performance. Furthermore, an algorithm-based estimation can serve as a weightless substitute or as feedback for robust control.

Manuscript received 16 February 2022; accepted 20 June 2022. Date of publication 12 July 2022; date of current version 21 July 2022. This letter was recommended for publication by Associate Editor M. Bangura and Editor P. Pounds upon evaluation of the reviewers' comments. This work was supported by JSPS KAKENHI under Grant JP20H05752. *(Corresponding author: Satoshi Suzuki.)*

Abner Asignacion, Satoshi Suzuki, Toshiyuki Nakata, and Hao Liu are with the Department of Mechanical Engineering, Chiba University, Chiba 263-8522, Japan (e-mail: abner_asignacion@yahoo.com; suzuki-s@chiba-u.jp; tnakata@chiba-u.jp; hliu@faculty.chiba-u.jp).

Ryusuke Noda is with the Department of Aeronautics and Astronautics, Kyoto University, Kyoto 615-8540, Japan (e-mail: noda.ryusuke.6a@kyoto-u.ac.jp).

Digital Object Identifier 10.1109/LRA.2022.3190073

A. Review of Related Works

Wind gust estimation, for either wind velocity or force/torque due to wind gusts, has been an emerging research topic over the past few years. Data-based approaches have been presented, in which the collected IMU data [2] or autopilot data [3] are used to estimate the wind velocity offline. In [4] and [5], wind velocity was estimated using a simple calculation based on the wind triangle principle. However, the estimation obtained using this technique heavily depends on the accuracy of the speed information obtained from both the ground frame and the inertial frame.

A model-based approach reported in [6] is capable of predicting the wind velocity with higher accuracy owing to the use of a trained model. However, this approach is only useful for that specific aircraft.

In [7], Kalman filters (KF) were developed for wind velocity estimation. The convergence rate for the KF is very low, and the accuracy is limited. In [8], an extended KF-based (EKF) approach was presented to estimate the airflow angles and the three-dimensional wind speed. However, it produced a sluggish estimation. In [9], an unscented KF-based method was proposed to estimate the external forces and torques acting on a quadrotor. The obtained results showed poor wrench estimation performance. The KF-based methods rely on stochastic assumptions, resulting in reduced accuracy during practical implementation.

Several works by *Tomic* et al. [10]–[12] proposed momentum and acceleration-based external wrench estimation. The developed technique was then patented in the US [13]. However, accurate measurement of acceleration in three dimensions is required. Acceleration-based approaches are popularized by *Leishman* et al. [14]. In [15], authors have utilized propeller induced drag to estimate the horizontal wind velocity. Using this drag model, wind gust are estimated using EKF with barometer [16] and with GPS [17]. *Bangura* et al. in [18] proposed a simple but state-of-the-art control and state estimation of attitude, inertial and body-fixed frame linear velocities that only requires IMU and barometer sensor systems. Additionally, when inertial measurements are available using GPS or vision system, it can estimate wind velocity as the offset between inertial and body-fixed frame linear velocities transformed into the same frame reference. However, the gains are tuned based on the stability condition and estimation performance but not wind characteristics.

Recent efforts utilize the well-known disturbance ob- servers (DOB) to estimate and compensate for the effects of wind gusts. DOB-based approaches are advantageous because they utilize only the system model and not the trained model. Moreover, these methods do not require additional sensors and stochastic assumptions. A high-gain extended state observer (ESO) was

proposed in [19] to estimate the turbulent wind gusts that disturbed the quadrotors flying in a defined trajectory. The obtained results had a high convergence rate owing to high gain. An unknown input observer (UIO), similar to the ESO, was used in [20]. However, the utilization of high gains resulted in overshooting. In summary, the existing DOB-based wind gust estimation methods focus on faster convergence that require higher gains. High-gain design leads to overshooting and results in wide bandwidths. Additionally, for a wide bandwidth, DOB estimates the wind disturbance considering uncertainties and other disturbances. Thus, the wind gust estimations are less accurate. To the best of the authors' knowledge, a frequency-based gain design and isolation of the wind gusts from the uncertainties and other disturbances have not been considered in previous studies.

B. Proposed Method and Contribution

This study proposes the first frequency-based estimation of the wind gusts using a DOB. More accurate wind gusts estimations can be obtained by considering the gust frequency range compared to the wind gusts estimations obtained using high gains. A nonlinear DOB (NDOB) is developed considering the frequency of the disturbance, which is similar to a conventional DOB (CDOB) [21]. This NDOB was first presented in [22], [23]. It aimed to replicate the simplicity of the CDOB design methodology, for nonlinear systems using the T-S fuzzy framework. The ESO works on a bandwidth that offers a high convergence rate, but the desired cut-off frequency cannot be explicitly set [19]. In the developed NDOB, the desired cut-off frequency is set by designing a circular region that bounds the condition for choosing the observer gain. Furthermore, compared with other DOB-based methods [19], [20], the developed NDOB approximates the usual twelfth-order nonlinear model to a sixth-order model. This significantly reduces the computational cost.

The remainder of this paper is organized as follows. Modeling is presented in Section II, and the proposed method is explained in Section III. The verification of the proposed method using simulations and experiments with a short discussion are given in Section IV.

II. Dynamic Model and Wind Disturbance

This section presents the quadrotor dynamic model developed by considering the wind gust frequency. The developed model provides highly accurate wind gust estimations.

A. Quadrotor Model With Input Disturbance

A quadrotor includes a rigid chassis with a cross-shaped structure where four independent rotors are mounted at each end. The speed of each rotor is determined by the inputs: force u_f and three torques $u_{\tau\phi}$, $u_{\tau\theta}$ and $u_{\tau\psi}$. The quadrotor configuration and the relationship between the inputs and rotor speeds are shown in the Fig. 1.

A quadrotor is a non-holonomic multi-input multi-output (MIMO) system with outputs including three position states (x, y and z), three orientation states (roll ϕ, pitch θ and yaw ψ), and the corresponding rates. Thus, the total number of states in the system is twelve. Using the laws of motion, the quadrotor

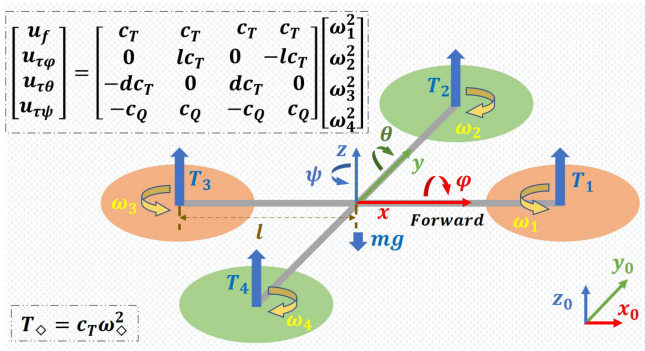

Fig. 1. Notation and the free-body diagram for the quadrotor equation of motion. The rotor thrust $T_\diamond$ is equivalent to the product of the thrust constant c_T and the square of the rotor speed $\omega_\diamond$. l is the arm length, c_Q is the drag constant that is used for determining the rotor speed.

system model in the presence of disturbance $d_\diamond$ is

$$\begin{aligned} m\ddot{x} &= (c(\phi)s(\theta)c(\psi) + s(\phi)s(\psi))\, u_f - k_x\dot{x} + d_x, \\ m\ddot{y} &= (c(\phi)s(\theta)s(\psi) - s(\phi)c(\psi))\, u_f - k_y\dot{y} + d_y, \\ m\ddot{z} &= -mg + (c(\phi)c(\theta))\, u_f - k_z\dot{z} + d_z, \\ J_\phi\ddot{\phi} &= (J_\theta - J_\psi)\,\dot{\theta}\dot{\psi} - k_\phi\dot{\phi}^2 + u_{\tau\phi} + d_\phi, \\ J_\theta\ddot{\theta} &= (J_\psi - J_\phi)\,\dot{\phi}\dot{\psi} - k_\theta\dot{\theta}^2 + u_{\tau\theta} + d_\theta, \\ J_\psi\ddot{\psi} &= (J_\phi - J_\theta)\,\dot{\phi}\dot{\theta} - k_\psi\dot{\psi}^2 + u_{\tau\psi} + d_\psi \end{aligned} \tag{1}$$

where m is the quadrotor's mass, g is the gravitational acceleration, $k_\diamond$ is the aerodynamic-positive constant, $J_\diamond$ is the rotary inertia constant and $s(\diamond)$ and $c(\diamond)$ are sine and cosines of the Euler angles, respectively.

The disturbance $d_\diamond$ includes the effects of the unmodeled dynamics $\Delta_\diamond$, wind gusts in terms of force/torque $w_\diamond$ and other disturbances $\kappa_\diamond$. The total disturbance can be expressed as,

$$d_\diamond = \Delta_\diamond + w_\diamond + \kappa_\diamond. \tag{2}$$

As the DOB estimates all disturbances with frequencies lower than the cut-off frequency, the obtained estimation includes the effects of wind disturbance and other disturbances. Hence, by determining and considering the frequency range of the wind gusts f_w, DOB estimates highly accurate wind gust data.

B. Wind Gust Disturbance

In [24], the frequency spectrum measurements of turbulence during relatively strong winds from approximately hundred meters above the surface of the earth were obtained. Multiple areas exhibited four similar distinct spectral peaks. Three of these peaks can be considered quasi-static. The rightmost peak had a frequency range of 0.005–0.1389 Hz, corresponding to the frequency range of the wind gusts f_w. *Tomic and Haddadin* in [11] performed spectrogram analyses and showed that the wind gusts act at a lower frequency than other disturbances (collisions). The wind gust frequency information was used only to differentiate the effects of the wind gusts from those of the collisions. Here, other disturbances $\kappa_\diamond$ cover all disturbance higher than f_w (e.g. collision).

In, [20], they suggested that the wind gusts are mainly horizontal and only affect the x and y dynamics substantially.

Whereas, the present study considers all the effects on the states, including the orientation states, demonstrating the generality and simplicity of the present approach. This study focuses on wind gusts estimation, excluding the controller design. Future work can focus on inclusion of a robust controller design to compensate for the disturbances.

III. Proposed Method

The problem with the existing observers for wind gust estimation is that the frequency is not considered or mentioned in the design. Therefore, in practice, these methods may experience inequalities in their estimation. On the other hand, the developed method considers frequency in the design process to obtain a reliable estimate of wind disturbance.

The dynamic model of the quadrotor is explicitly nonlinear. Hence, employing a linear model without the hovering condition for the design of a DOB significantly increases the unmodelled dynamics in the unknown frequency ranges. Therefore, a nonlinear disturbance observer (NDOB) must be used. The nonlinear model described in (1) is thus utilized.

A. T-S Fuzzy NDOB

Consider the nonlinear dynamics model as described below,

$$\dot{X} = a(X,t) + b(X,t)U + b_d(X,t)D \tag{3}$$

where X is the state vector, U is the input vector, D is the disturbance vector and $a(X,t)$, $b(X,t)$ and $b_d(X,t)$ are nonlinear expressions for the state, input and disturbance, respectively. This can be approximated in the T-S fuzzy framework [25] as a group of δ linear sub-models.

$$\dot{X} = \sum_{i=1}^{\delta} h_i(X)\left(A_i X + B_i U + B_{di} D\right) \tag{4}$$

where A_i, B_i and B_{di} are matrices with appropriate sizes. Furthermore, $h_i(X)$ are the membership functions which can be described as follows,

$$\sum_{i=1}^{\delta} h_i(X) = 1. \tag{5}$$

This means that the membership function determines the extent to which a certain linear sub-model can affect the entire T-S fuzzy model. The number of membership functions or sub-models δ depends on the number of the states ζ that causes nonlinearity in $a(X,t)$, $b(X,t)$ and $b_d(X,t)$ as given below,

$$2^{\zeta} = \delta. \tag{6}$$

Two static values for each state are considered, which exhibit linear characteristics to create a linear sub-model.

Here, the output is assumed to be linearly described by the state vector as given below,

$$Y = CX. \tag{7}$$

Subsequently, a state observer in the T-S fuzzy framework is expressed as given below,

$$\dot{\widehat{X}} = \sum_{i=1}^{\delta} h_i(X)\left\{A_i \widehat{X} + B_i U + L_i C\left(X - \widehat{X}\right)\right\} \tag{8}$$

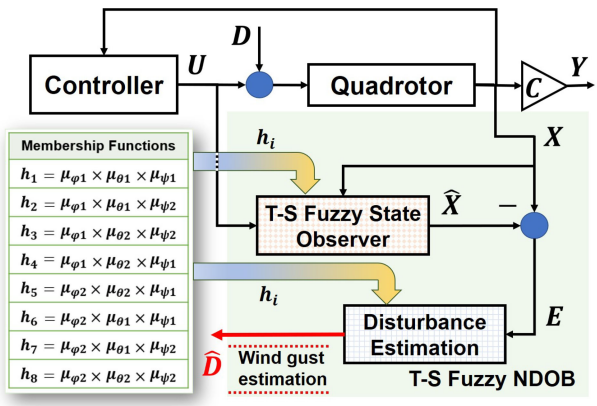

Fig. 2. Structure of T-S fuzzy NDOB for the wind gust estimation with the membership functions. $\mu_{\diamond}$ is described in (16).

By subtracting eqs. (4) and (8), the error dynamics can be easily obtained as follows,

$$\dot{E} = \sum_{i=1}^{\delta} h_i(X)\left\{\left(A_i - L_i C\right)E + B_{di} D\right\}. \tag{9}$$

To guarantee the convergence of the above-mentioned error dynamics, consider this Lyapunov candidate function $V(t) = 0.5E^T Q E > 0$. Furthermore, the rate of change of $V(t)$ is

$$\dot{V}(t) = A_i Q + Q A_i^T - H_i^T C - C^T H_i < 0 \tag{10}$$

where $H_i = L_i^T Q$. The rate of convergence f_E is determined by the observer gain L_i, which is designed using the LMI pole-placement method. In [26], an LMI pole-placement method for control was developed. The method can be transformed for the observer design using (10), resulting in a MATLAB solvable LMI as given below,

$$\begin{bmatrix} -rQ & cQ + A_i Q - H_i^T C \\ cQ + Q A_i^T - C^T H_i & -rQ \end{bmatrix} < 0. \tag{11}$$

where r and c are the radius and the center of the circular region where the poles are placed, respectively, as shown in the Fig. 3. If the system described in (3) stabilizes with any controller and by solving the above-mentioned LMI, then the error E converges to zero. This guarantees the stability of the whole system.

If the rate of convergence f_E of the error dynamics E is faster than the frequency of the disturbance f_D, then $\dot{E} = 0$. Furthermore, the disturbance can be algebraically computed using (9) as follows,

$$\hat{D} = -\sum_{i=1}^{\delta} h_i(X)\left\{\left(B_{di}^T B_{di}\right)^{-1} B_{di}^T \left(A_i - L_i C\right) E\right\}. \tag{12}$$

The proposed approach is shown in Fig. 2, where the T-S fuzzy state observer is as given by (8), and the disturbance estimation is as described in (12).

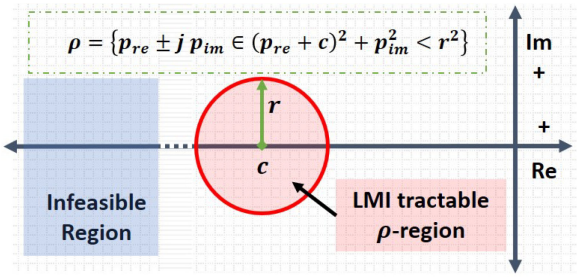

Fig. 3. The design parameters r and c place the poles in a circular region at the left side of the complex plane that are obtained using the LMI pole-placement method. The design must consider the possibility of infeasibility if the chosen c is too high.

B. T-S Fuzzy NDOB for Quadrotors

The virtual control inputs are used and selected as described below to solve the under-actuation problem.

$$\begin{aligned} v_1 &= (c(\phi)s(\theta)c(\psi) + s(\phi)s(\psi))\, u_f/m, \\ v_2 &= (c(\phi)s(\theta)s(\psi) - s(\phi)c(\psi))\, u_f/m, \\ v_3 &= -g + (c(\phi)c(\theta))u_f/m. \end{aligned} \tag{13}$$

Here, a sixth-order system was utilized to reduce the computational cost. Based on (1), the system model can be described using the following matrices,

$$\begin{aligned} X &= \begin{bmatrix} \dot{x} & \dot{y} & \dot{z} & \dot{\phi} & \dot{\theta} & \dot{\psi} \end{bmatrix}^T, \\ U &= \begin{bmatrix} v_1 & v_2 & v_3 & \frac{u_{\tau\phi}}{J_\phi} & \frac{u_{\tau\theta}}{J_\theta} & \frac{u_{\tau\psi}}{J_\psi} \end{bmatrix}^T, \\ D &= \begin{bmatrix} \frac{d_x}{m} & \frac{d_y}{m} & \frac{d_z}{m} & \frac{d_\phi}{J_\phi} & \frac{d_\theta}{J_\theta} & \frac{d_\psi}{J_\psi} \end{bmatrix}^T, \\ a(X,t) &= \begin{bmatrix} \frac{-k_x}{m} & \frac{-k_y}{m} & \frac{-k_z}{m} & a_4 & a_5 & a_6 \end{bmatrix}^T, \\ b(X,t) &= b_d(X,t) = C = I_{6\times 6} \end{aligned} \tag{14}$$

where $a_4 = \frac{(J_\theta - J_\psi)\dot{\theta}\dot{\psi} - k_\phi \dot{\phi}^2}{J_\phi}$, $a_5 = \frac{(J_\psi - J_\phi)\dot{\phi}\dot{\psi} - k_\theta \dot{\theta}^2}{J_\theta}$, $a_6 = \frac{(J_\phi - J_\theta)\dot{\phi}\dot{\theta} - k_\psi \dot{\psi}^2}{J_\psi}$ and I is an identity matrix. Note that $b(X,t)$ and $b_d(X,t)$ are linear, and only $a(X,t)$ shows nonlinearity.

According to (6), there are eight membership function ($\delta = 8$). This is because there are only three states ($\zeta = 3$) that cause nonlinearity in $a(X,t)$. The fuzzy rules to transform this nonlinear system into a T-S fuzzy model are as follows,

$$\begin{aligned} &\text{Rule } i\text{: IF } \dot{\phi} \text{ is } \dot{\phi}_i, \\ &\quad \text{and IF } \dot{\theta} \text{ is } \dot{\theta}_i, \\ &\quad \text{and IF } \dot{\psi} \text{ is } \dot{\psi}_i, \\ &\quad \text{THEN } \dot{x} = A_i x + BU + BD \end{aligned}$$

where $\diamond_i$ are the constant minimum and maximum values of the angular rates and i is the rule number, which are shown in Table I. Subsequently, the membership functions as shown in Fig. 2 are determined as given below,

$$h_i = \mu_{\phi\diamond} \times \mu_{\theta\diamond} \times \mu_{\psi\diamond} \tag{15}$$

TABLE I
STATIC VALUES OF THE ANGULAR RATES FOR THE FUZZY RULES

Rule no.	$\dot{\phi}$	$\dot{\theta}$	$\dot{\psi}$
1	$\dot{\phi}_{min}$	$\dot{\theta}_{min}$	$\dot{\psi}_{min}$
2	$\dot{\phi}_{min}$	$\dot{\theta}_{min}$	$\dot{\psi}_{max}$
3	$\dot{\phi}_{min}$	$\dot{\theta}_{max}$	$\dot{\psi}_{max}$
4	$\dot{\phi}_{min}$	$\dot{\theta}_{max}$	$\dot{\psi}_{min}$
5	$\dot{\phi}_{max}$	$\dot{\theta}_{max}$	$\dot{\psi}_{min}$
6	$\dot{\phi}_{max}$	$\dot{\theta}_{min}$	$\dot{\psi}_{min}$
7	$\dot{\phi}_{max}$	$\dot{\theta}_{min}$	$\dot{\psi}_{max}$
8	$\dot{\phi}_{max}$	$\dot{\theta}_{max}$	$\dot{\psi}_{max}$

where $\diamond$ is 1 denotes maximum, while a value of 2 for $\diamond$ denotes minimum. The expression is as given below,

$$\begin{aligned} \mu_{\circ 2} &= \frac{\circ - \circ_{min}}{\circ_{max} - \circ_{min}}, \\ \mu_{\circ 1} &= 1 - \mu_{\circ 2} \end{aligned} \tag{16}$$

where $\circ$ are angular rates. Subsequently, following the structure shown in Fig. 2, the T-S fuzzy state observer can be developed as in (8). Furthermore, the disturbance can be estimated using (12). The estimated disturbance includes all the disturbances with a frequency f_D lower than the convergence rate f_E.

C. Frequency-Based Design

By considering the frequency of wind gusts, a frequency-based design for wind gust estimation can yield a more accurate estimate. Here, the T-S fuzzy NDOB, although nonlinear, can be designed by considering the disturbance frequency.

1) Comparison of Two Linear DOBs: Using eqs. (9) and (12), a new state-space model is developed, where the state vector is the error vector E, the input vector is the disturbance D and the output vector is the estimated disturbance $\hat{D}$. Without the T-S fuzzy framework (i.e. only considering a linear system), the transfer function is obtained using the following.

$$G_{D-\hat{D}} = C_E(sI - A_E)^{-1}B_d \tag{17}$$

where $A_E = A - LC$ and $C_E = -(B_d^T B_d)^{-1}B_d^T(A - LC)$.

To simplify the discussion, the conventional DOB (CDOB) and state-space DOB (SSDOB) [23] were utilized on a linear system $P(s)$. The comparison is as shown in Fig. 4. The SSDOB is the linear version of the proposed NDOB. With the same equivalent system model, CDOB employs a nominal model, whereas SSDOB utilizes a state observer. Both the CDOB and SSDOB contain the nominal dynamics of the system. The frequency responses of the $Q(s)$ and $G_{D-\hat{D}}$, which determine the frequency range of the disturbance estimation, are the same. By placing the poles at f_c, it can be verified that the SSDOB is equivalent to the CDOB in a different form.

2) Frequency Analysis of Proposed NDOB: SSDOB is extended to the nonlinear systems by using the T-S fuzzy framework. The frequency response of a T-S fuzzy model can be illustrated using the fuzzy frequency response (FFR), which was introduced in [27] and is as shown in the Fig. 5(b). According to the FFR, the nonlinear system frequency response is bounded by the sub-models of the T-S fuzzy model, and each linear sub-model has a distinct frequency response plot.

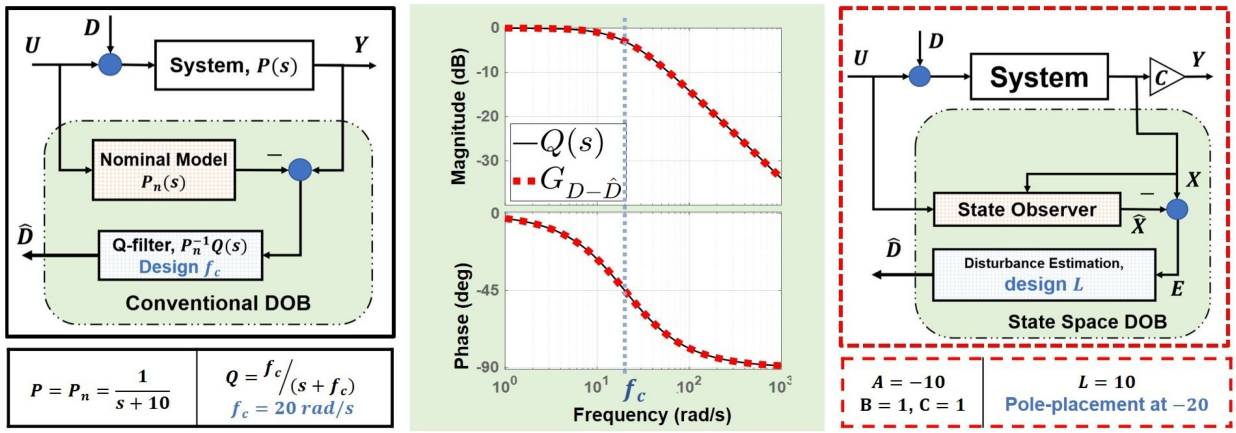

Fig. 4. Comparison of the CDOB and SSDOB in terms of the structure, frequency response and design approach. The former is designed by choosing an appropriate cut-off frequency f_c while the latter uses a pole-placement to achieve the same f_c.

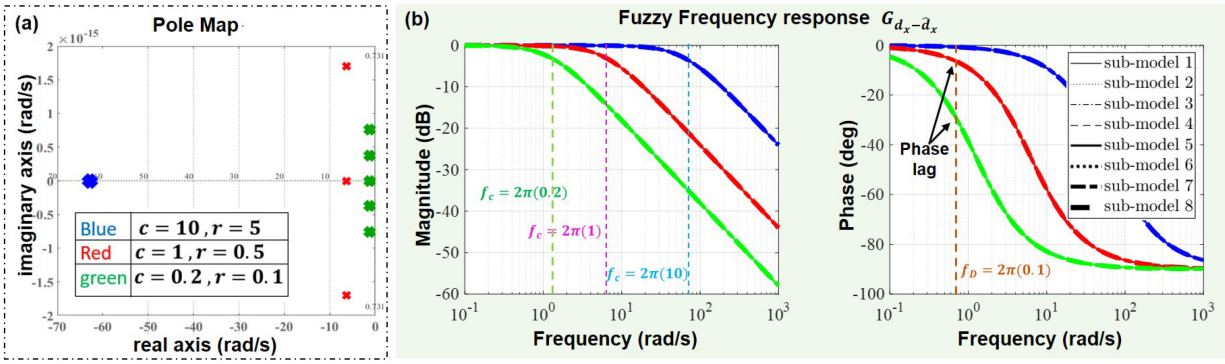

Fig. 5. (a) Pole Map and (b) FFR for the T-S fuzzy NDOB. The system parameters are stated in Section IV. The color legend from the Pole Map applies to the FFR.

However, in Fig. 5(b), FFR of $G_{d_x-\hat{d}_x}$, which describes the disturbance affecting x position, shows the coinciding frequency responses of the 8 sub-models. The pole map is as shown in the Fig. 5(a). This map helps to check the distance between the poles. The poles close to each other produce coinciding Bode plots. In the present study, the obtained poles were observed to be almost coincident (the imaginary axis range was $\times 10^{-15}$). Consequently, the cut-off frequency f_c of the T-S fuzzy model can be easily determined as $2\pi c$. Furthermore, in this case, the rate of convergence f_E is close to f_c.

$$f_E \approx f_c \tag{18}$$

With system model in (1), any cut-off frequency results in coinciding frequency responses. However, this is not always the case for other systems or complex quadrotor models since a complex model can lead to a dispersed pole placement inside the circular region. In addition to this, the pole placement can create zeros that affect the frequency response, especially if they are created on the right side (using the pole–zero map) of the poles. This type of NDOB was first presented in [22]. Additionally, its comparison with the other DOBs was also discussed.

The design of the cut-off frequency f_c of the DOB must consider the frequency range of the wind gusts f_w. Note that f_c is the frequency at which a significant phase lag is observed, as shown in the Fig. 5(b). The magnitude is important for the estimation. However, the phase is unimportant because it is not used as an input in the feedback loop. Therefore, f_c can be chosen that is close to f_w. This study considered $f_c = 1$ Hz $(c = 1, r = 0.5)$.

IV. Results and Discussion

This section verifies the proposed method by determining its wind gust estimation performance.

A. MATLAB/Simulink Simulation

An SJTU drone developed by Shanghai Jiao Tong University (SJTU) was used to perform the simulations in MATLAB/Simulink. The parameters are as follows: $m = 1.477$ kg, $k_\diamond = 5.5\times10^{-}4$ N.m.s, $J_\phi = J_\theta = 0.1152$ kg.m ^{2} and $J_\psi = 0.218$ kg.m^2. The chosen static value, as mentioned in previous section, are chosen as min $= -10$ rd/ s and max $= 10$ rd / s for all angular rates.

For all simulations, the quadrotor followed an upward spiral track, and the wind gust frequency f_D was set to 0.1 Hz which is inside the frequency range of wind gusts f_w.

Initially, the proposed method was verified using MATLAB/Simulink with SJTU drone parameters. For the T-S fuzzy

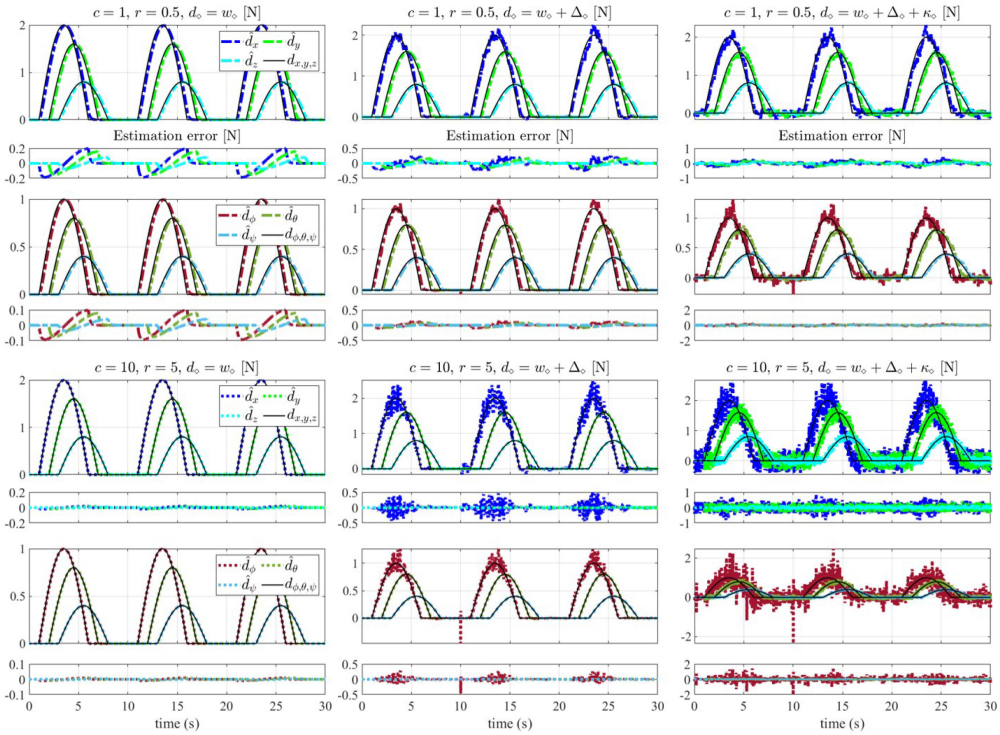

Root Mean Square Error (RMSE)

$c = 1, r = 0.5$

$\hat{d}_\diamond$	col 1	col 2	col 3
x	0.096	0.110	0.131
y	0.077	0.077	0.098
z	0.038	0.038	0.049
φ	0.048	0.055	0.074
θ	0.038	0.038	0.049
ψ	0.019	0.019	0.025

$c = 10, r = 5$

$\hat{d}_\diamond$	col 1	col 2	col 3
x	0.038	0.126	0.235
y	0.008	0.008	0.158
z	0.004	0.004	0.077
φ	0.005	0.056	0.251
θ	0.004	0.004	0.079
ψ	0.002	0.002	0.039

Fig. 6. MATLAB/Simulink performance comparison of the proposed method using two different design parameters under three disturbance conditions. The odd rows are the disturbance estimation. The even rows represent the estimation error of the preceding odd row. The RMSE values are provided at the right.

state observer, the state matrix becomes

$$A_i = \begin{bmatrix} A_{\alpha i} & 0_{3\times 3} \\ 0_{3\times 3} & A_{\beta i} \end{bmatrix}.$$

$$A_{\alpha i} = \begin{bmatrix} \alpha_1 & 0 & 0 \\ 0 & \alpha_2 & 0 \\ 0 & 0 & \alpha_3 \end{bmatrix}, \quad A_{\beta i} = \begin{bmatrix} \alpha_4 & 0 & \beta_4 \\ 0 & \alpha_5 & \beta_5 \\ \beta_6 & 0 & \alpha_6 \end{bmatrix}$$

where $\alpha_1 = -k_x/m$, $\alpha_2 = -k_y/m$, $\alpha_3 = -k_z/m$, $\alpha_4 = -k_\phi\phi/J_\phi$, $\alpha_5 = -k_\theta\theta/J_\theta$, $\alpha_6 = -k_\psi\psi/J_\psi$, $\beta_4 = \frac{(J_\theta - J_\psi)\dot{\theta}}{J_\phi}$, $\beta_5 = \frac{(J_\psi - J_\phi)\dot{\phi}}{J_\theta}$ and $\beta_6 = \frac{(J_\phi - J_\theta)\dot{\theta}}{J_\psi}$. The dynamic states $\dot{\phi}$, $\dot{\theta}$ and $\dot{\psi}$ are changed to the static values as shown in Table I. Given that C is an identity matrix, the observer gain was easily obtained using LMI pole-placement method as follows

$$L_i = \begin{bmatrix} L_{\alpha i} & 0_{3\times 3} \\ 0_{3\times 3} & L_{\beta i} \end{bmatrix}.$$

$$L_{\alpha i} = \begin{bmatrix} \iota_1 & 0 & 0 \\ 0 & \iota_2 & 0 \\ 0 & 0 & \iota_3 \end{bmatrix}, \quad L_{\beta i} = \begin{bmatrix} \iota_4 & 0 & \beta_4 \\ 0 & \iota_5 & \beta_5 \\ \beta_6 & 0 & \iota_6 \end{bmatrix}$$

where $\iota_j = f_c - \alpha_j$ for $j = 1, 2 \ldots 6$.

As shown in Fig. 6 and considering (2), three disturbance conditions (DC1: $d_\diamond = w_\diamond$, DC2: $d_\diamond = w_\diamond + \Delta_\diamond$ and DC3: $d_\diamond = w_\diamond + \Delta_\diamond + \kappa_\diamond$) are considered to evaluate the wind gust estimation performance of the proposed method. Whereas, these two different design parameters (DP1: $c = 1$, $r = 0.5$, DP2: $c = 10$, $r = 5$) are considered. The FFR plots of these design parameters are shown in Fig. 5(b). In the first column (DC1), the disturbance affecting the quadrotor is a wind gust with magnitude $W_\diamond = \{2, 1.6, 0.8, 1, 0.8, 0.4\}$ which is described as

$$w_\diamond = \begin{cases} W_\diamond \sin(2\pi f_D), & W_\diamond \geq 0 \\ 0, & W_\diamond < 0 \end{cases} \tag{19}$$

The estimation obtained in DP1 is more accurate than that in DP2 because of its faster convergence or higher cut-off frequency. The DP1 estimation does not coincide with the actual disturbance, unlike that of DP2. The RMSE was higher in DP1 than in DP2 because of the phase lag. Note that the magnitude is the same, and only the phase lag causes a significant estimation error. The FFR is as shown in Fig. 5(b). A phase lag of approximately 5.7° for $f_c = 1$ Hz and $f_D = 0.1$ Hz is obtained. However, DOB with a higher cut-off frequency estimates a wider frequency range. Thus, it includes other unnecessary disturbances.

In the second column (DC2) of Fig. 6, the total disturbance of x dynamics (d_x) and ϕ dynamics (d_ϕ) include both wind gusts w and uncertainties Δ. These uncertainties are introduced by multiplying the x and ϕ dynamics by $1 + \lambda$ (λ is uniform random signal with $\{-0.2, 0.2\}$ range and frequency of 100 rd / sec).). It is clear that the estimation in DP2 is less accurate and has a higher RMSE than that in DP1. The RMSE values in DC2 for the other states are the same as those in DC1. This is because there are no uncertainties added to these states.

The advantage of DP1 becomes more apparent when other disturbance $\kappa_\diamond$ is added to the total disturbance $d_\diamond$, as shown in the third column (DC3). $\kappa_\diamond$ affects all dynamics and is given as a uniform random signal with $\{-0.5, 0.5\}$ range and frequency of 50 rd / sec, which is higher than f_w. The estimation in DP1 was far better than that obtained in DP2, which is also observed from the RMSE values presented in Fig. 6.

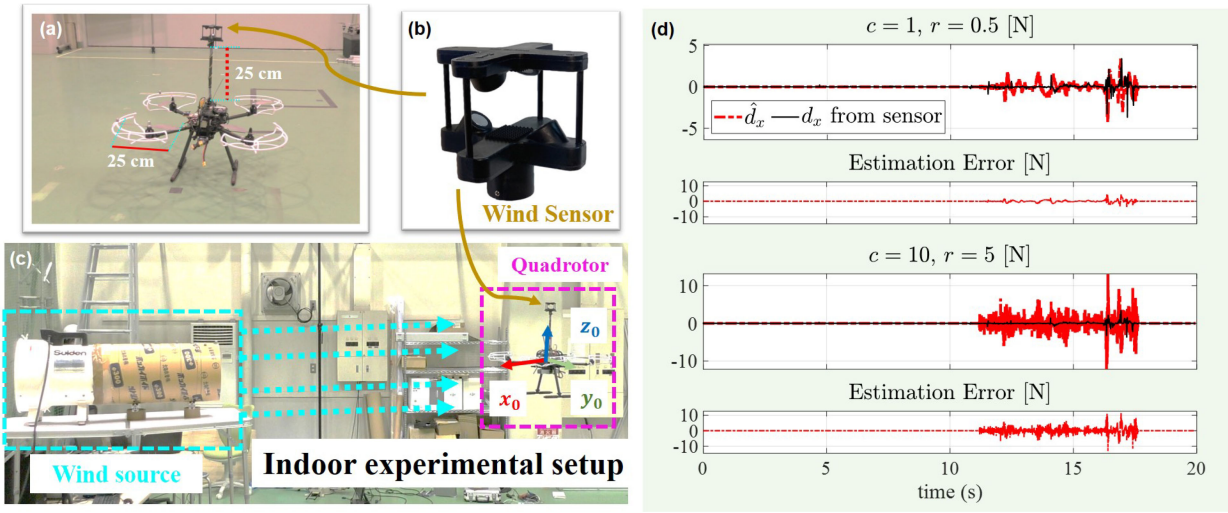

Fig. 7. (Experiment) : (a) 2.5 kg quadrotor, (b) wind sensor, (c) experimental setup, and (d) performance comparison of the proposed method obtained using two different design parameters.

It can be verified from these simulation results that choosing a lower cut-off frequency produces a more accurate wind gust estimation when the quadrotor is affected by other disturbances.

B. Experimental Verification

The present section discusses the verification of the proposed method with the experimental results using a 2.5 kg quadrotor, with the following parameters: $J_\phi = 0.055$ kg.m^2, $J_\theta = 0.05$ kg.m^2, $J_\psi = 0.0642$ kg.m^2 and $k_\diamond$ is negligible. The quadrotor is equipped with a TriSonica Mini wind sensor (as in [28]) at 25 cm (same as the propeller blade length) above the quadrotor, as shown in the Figs. 7(a) and (b). This wind sensor can accurately measure the wind velocity in the x and y directions. The sampling rate of the control program and sensor data was set to 50 Hz. Parametric uncertainties exist for all the inertia values owing to the placement of the sensor (50 g). The quadrotor was operated freely, without track planning.

The experiment was performed indoors where the quadrotor is affected by a wind source (maximum wind velocity of 8 m/s) in x direction, as illustrated in Fig. 7(c). The wind force $w_\diamond$ was calculated by using the air density $\rho_w = 1.225$ kg/m^3, affected quadrotor's surface area S_A and wind velocity $v_\diamond$ using the following expression, $w_\diamond = \rho_w S_A v_\diamond^2$. A video is provided online.[1]

The wind source is assumed to provide a constant wind speed. The wind measurements and estimation depend on the quadrotor's position with respect to the area affected by the wind source. When the quadrotor is in the area of effect of the wind source, the wind force is positive, and it pushes the quadrotor back. The wind force becomes negative when the quadrotor moves out of the affected area. This is followed by the quadrotor moving forward owing to inertial effects. There is no significant wind source along the y-direction. In Fig. 7(d), DP1 provided a better estimation performance than DP2. In other words, less estimation error was obtained in DP1 (RMSE $= 0.43$) than in DP2 (RMSE $= 1.03$).

[1][Online]. Available: https://youtu.be/wG8oFhunNMA

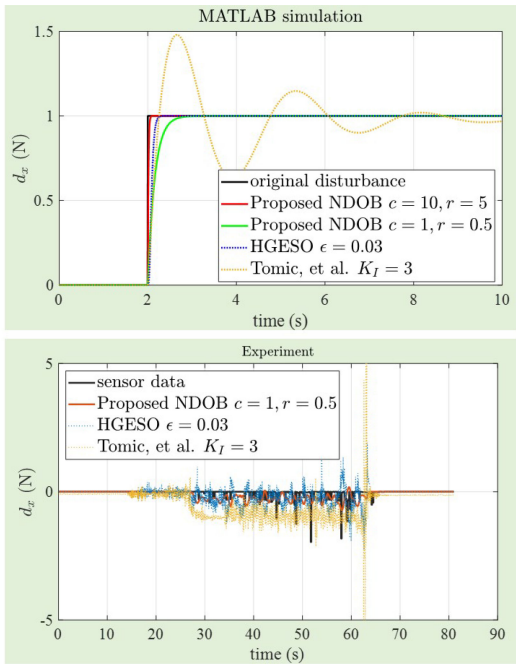

Fig. 8. Comparison of the simulation and experimental results showing the estimation performance of various wind gust estimation methods.

C. Discussion

The wind frequency used for the simulations was in the higher range of f_w, whereas in the experiment, it was expected to be in the range of f_w. Wind disturbances with a frequency lower than f_c are expected to be estimated accurately, following a frequency response similar to that of a low-pass filter.

The comparison of the proposed method with the existing observers for wind gust estimation, in terms of estimation performance is an important point of discussion. However, a useful performance comparison requires the optimal design for each approach. Herein, we consider the design parameters as discussed in the previous studies. In Fig. 8, a comparison of the

HGESO approach (as discussed in [19]) and the acceleration-based approach proposed by Tomic *et al.* [10]–[12] is presented. The HGESO requires the position and orientation data, along with a design parameter ϵ while the acceleration-based approach requires acceleration data and the design parameter K_I. Our approach requires the rate information along with the design parameters c and r for cut-off frequency f_c. MATLAB differentiation is used to obtain the rates and the acceleration data. The simulation was carried out using a step wind disturbance. Compared to our approach with $c = 1$ and $r = 0.5$, the HGESO has a faster response owing to its high gain, while the acceleration-based approach has a slower response. In the experiment,[2] it is observed that the HGESO shows higher inaccuracy as compared to the developed approach. This is due to the modeling errors and inconsideration of wind gust frequency. Additionally, high accuracy results are obtained using the developed method as compared to those obtained using the acceleration-based approach. This is because the results obtained using the acceleration-based approach rely on the accuracy of the accelerometer.

The main strength of the developed approach is the consideration of the frequency, although quadrotors are nonlinear. A high cut-off frequency results in faster wind gust estimation. However, in practice, less accurate wind gust estimations are obtained due to the existence of uncertainties and other disturbances. Furthermore, the developed method is more general and not limited to quadrotors. It can also be used in any UAVs for wind gust estimation. Moreover, it only requires a standard sensor suit for the UAVs, and no additional sensors are needed.

V. Conclusion and Future Work

The present study proposed an active wind gust estimation method using a T-S fuzzy based nonlinear DOB that can focus on the wind gust frequency. By choosing an appropriate NDOB cut-off frequency, it was verified that the other disturbances and modeling errors were significantly attenuated, and a more accurate wind gust estimation was predicted. The proposed method was validated with the simulations and the experimental results with the help of the estimation performance comparison between different cut-off frequencies and other estimation methods.

Future work would include a robust control design and the noise reduction for compensating for the disturbances and improving the estimation as well as the tracking performance. Moreover, it would also consider the noise affecting the wind gust estimation and feedback control. Furthermore, the aerodynamic effects of the quadrotor propeller will also be studied in detail. Lastly, the possibility of different frequency range of highly turbulent wind condition will be dealt in the future work.

References

[1] D. Tripp, E. Martin, and H. Reeves, "Applications of unscrewed aerial vehicles (UAVs) in winter precipitation-type forecasts," *J. Appl. Meteorol. Climatol.*, vol. 60, no. 3, pp. 361–375, Mar. 2021.

[2] M. Mazzatenta, D. Carter, and Q. Daniel, "Using quadrotor IMU data to estimate wind velocity," *APS Division Fluid Dyn.*, vol. 64, no. 13, pp. 777–780, 2019.

[3] M. Simma, H. Mjøen, and T. Boström, "Measuring wind speed using the internal stabilization system of a quadrotor drone," ,*Drones*, vol. 4, no. 2, 2020, Art. no. 23.

[4] P. P. Neumann and M. Bartholmai, "Real-time wind estimation on a micro unmanned aerial vehicle using its inertial measurement unit," *Sens. Actuators A. Phys*., vol. 235, pp. 300–310, 2015.

[5] S. Mayer, Stephanie, G. Hattenberger, P. Brisset, M. O. Jonassen, and J. Reuder, "A 'no-flow-sensor' wind estimation algorithm for unmanned aerial systems," *Int. J. Micro Air Veh.*, vol. 4, no. 1, pp. 15–29, 2012.

[6] J. Gonzalez-Rocha, C. A. Woolsey, C. Sultan, S. D. Wekker, and N. Rose, "Measuring atmospheric winds from quadrotor motion," in *Proc. AIAA Atmospheric Flight Mechanics Conf.*, 2017, pp. 9–13.

[7] K. T. Borup, B. N. Stovner, T. I. Fossen, and T. A. Johansen, "Kalman filters for air data system bias correction for a fixed-wing UAV," *IEEE Trans. Control Syst. Tech.*, vol. 28 no. 6, pp. 2164–2176, Nov. 2020.

[8] A. Cho, Y.-S. Kang, B.-J. Park, and C.-S. Yoo, "Airflow angle and wind estimation using GPS/INS navigation data and airspeed," in *Proc. IEEE 13th Int. Conf. Control, Automat. Syst.*, 2013, pp. 1321–1324.

[9] C. D. McKinnon and A. Schoellig, "Unscented external force and torque estimation for quadrotors," in *Proc. IEEE/RSJ Int. Conf. Intell. Robots Syst.*, 2016, pp. 5651–5657.

[10] T. Tomić and S. Haddadin, "A unified framework for external wrench estimation, interaction control and collision reflexes for flying robots," in *Proc. IEEE/RSJ Int. Conf. Intell. Robots Syst.*, 2014, pp. 4197–4204.

[11] T. Tomic and S. Haddadin, "Simultaneous estimation of aerodynamic and contact forces in flying robots: Applications to metric wind estimation and collision detection," in *Proc. IEEE Int. Conf. Robot. Autom.*, 2015, pp. 5290–5296.

[12] T. Tomić, C. Ott, and S. Haddadin, "External wrench estimation, collision detection, and reflex reaction for flying robots," *IEEE Trans. Robot.*, vol. 33, no. 6, pp. 1467–1482, Dec. 2017.

[13] T. Tomic, P. Lutz, and S. Haddadin, "Wind measurement by means of a multicopter," .U.S. Patent 11,214,366, Jan. 4, 2022.

[14] R. C. Leishman, J. C. Macdonald, R. W. Beard, and T. W. McLain, "Quadrotors and accelerometers: State estimation with an improved dynamic model," *IEEE Control Syst. Mag.*, vol. 34, no. 1, pp. 28–41, Feb. 2014.

[15] S. L. Waslander and C. Wang, "Wind disturbance estimation and rejection for quadrotor position control," in *Proc. AIAA Infotech, Aerosp. Conf.*, 2009, Art. no. 1983.

[16] M. Burri, M. Datwiler, M. W. Achtelik, and R. Siegwart, "Robust state estimation for micro aerial vehicles based on system dynamics," in *Proc. IEEE Int. Conf. Robot. Automat.*, 2015, pp. 5278–5283.

[17] L. N. C. Sikkel, G. C. H. E. De Croon, C. De Wagter, and Q. P. Chu, "A novel online model-based wind estimation approach for quadrotor micro air vehicles using low cost MEMS IMUS," in *Proc. IEEE Intell. Robots Syst.*, 2016, pp. 2141–2146.

[18] M. Bangura, X. Hou, G. Allibert, R. Mahony, and N. Michael, "Supervisory control of multirotor vehicles in challenging conditions using inertial measurements," *IEEE Trans. Robot.*, vol. 34, no. 6, 1490–1501, Dec. 2018.

[19] A. Miranda-Moya, H. Castañeda, and H. Wang, "Turbulent wind gusts estimation and compensation via high-gain extended observer-based adaptive sliding mode for a quadrotor UAV," in *Proc. IEEE Int. Conf. Unmanned Aircr. Syst.*, 2021, pp. 476–481.

[20] S. I. Azid, K. Kumar, M. Cirrincione, and A. Fagiolioni, "Robust motion control of nonlinear quadrotor model with wind disturbance observer," *IEEE Access*, vol. 9, pp. 149164–149175, Nov. 2021.

[21] W. Chen, J. Yang, L. Guo, and S. Li, "Disturbance-observer-Based control and related methods–An overview," *IEEE Trans. Ind. Electron.*, vol. 63, no. 2, pp. 1083–1095, Feb. 2016.

[22] A. Asignacion, "T-S fuzzy disturbance observer based on frequency response," Ph.D. Dissertation, Dept. Elec. Eng., Changwon National Univ., South Korea, 2019. Accessed: Jul. 14, 2022. [Online]. Available: https://drive.google.com/file/d/1Uvw_wyXKA6IFnqzhflXxlUOycg2x6L-A/view?usp=sharing

[23] S. Park and T. S. Yoon, "State space disturbance observer considering residual disturbance," *IEEE Access*, vol. 8, pp. 213882–213886, 2020.

[24] S. Watkins, M. Thompson, B. Loxton, and M. Abdulrahim, "On low altitude flight through the atmospheric boundary layer," *Int. J. Micro Air Veh.*, vol. 2, no. 2, pp. 55–68, Jun. 2010.

[25] T. Takagi and M. Sugeno, "Fuzzy identification of systems and its applications to modeling and control," *IEEE Trans. Sys., Man, Cybern*., vol. 1, no. 15, pp. 116–132, Jan./Feb. 1985.

[26] S. K. Hong and Y. Nam, "Stable fuzzy control system design with pole-placement constraint: An LMI approach," *Comput. Ind.*, vol. 51, no. 1, pp. 1–11, 2003.

[27] C. C. T. Ferreira and G. L. O. Serra, "Fuzzy frequency response: Proposal and application for uncertain dynamic systems," *Eng. Appl. Artif. Intell.*, vol. 24, pp. 1186–1194, 2011.

[28] Anemoment LLC, "TriSonica mini wind and weather sensor." Accessed: Jul. 14, 2022. [Online]. Available: Available: anemoment.com/features/

[2][Online]. Available: https://youtu.be/VDFcm9blRCA